Nanoflowers

DOI: 10.1002/anie.201000902

A Universal Approach to the Synthesis of Noble Metal Nanodendrites and Their Catalytic Properties**

Ashok Mohanty, Niti Garg, and Rongchao Jin**

In the ever-expanding field of nanomaterials research, noble metal nanoparticles have received particular interest because of their fascinating properties and potential applications in catalysis, electronics, sensing, photonics, imaging, and biomedicine.[1] The shape-dependent properties of nanoparticles have stimulated research into noble metal nanoparticles of various shapes, such as nanorods or nanowires, nanocubes, nanoprisms, nano-octahedra and tetrahedra, nanoplates, and nanoflowers or nanostars.[1,2] Our interest focuses on star- or flower-shaped nanoparticles because their surface roughness and possible high-index facets could be utilized for surface-sensitive applications, such as catalysis and surface-enhanced Raman scattering (SERS). In fact, star-shaped gold nanoparticles are very efficient for SERS[2,3] and electrochemical applications[4] and also gyromagnetic imaging.[5] Similarly, Pt and Pd nanoflowers are excellent catalysts for the reduction of ferricyanide by thiosulfate,[6] methanol electro-oxidation,[7] and as electrocatalysts in polymer-electrolyte membrane fuel cells.[8,9] The superior catalytic activity of the flower-shaped nanoparticles stems from the exposure of certain high-index facets that are intrinsically more active towards specific reactions. For example, in the benzene hydrogenation reaction, Pt(100) produces only cyclohexane, whereas Pt(111) produces cyclohexane and cyclohexene.[10] Despite these superior properties, the synthesis of noble metal nanoflowers (or nanodendrites) with high degrees of structural anisotropy and having highly active facets on their surface is still a challenge, because nanoparticles tend to acquire shapes in which the surface is covered by low-index {100} and {111} facets favored by a lower surface energy.[11] Only a few reports are known for high-yield synthesis of noble metal nanoflowers with active facets,[2–9,12] and these works are mainly based on a seeding growth approach. In particular, to develop wet chemistry approaches, a universal method for synthesizing nanoflowers of noble metals is therefore highly desirable.

Herein, we report a universal approach for one-pot, high-yield synthesis of nanoflowers of Au, Pd, and Pt using an amino acid based surfactant, sodium *N*-(4-*n*-dodecyloxybenzoyl)-L-isoleucinate (SDBIL; Supporting Information, Figure S1). High-resolution transmission electron microscopy (HRTEM) studies in conjunction with selected-area electron-diffraction (SAED) and X-ray diffraction (XRD) methods reveal that the nanoflowers have high-index facets (e.g., {220} and {311}) that could be utilized to attain enhanced catalytic activity.

The Suzuki–Miyaura and the Heck coupling reactions are two important noble-metal-catalyzed processes for forming C–C bonds to produce medicines, agrochemicals, and fragrances.[13,14] The Suzuki–Miyaura coupling reaction is generally catalyzed by Pd nanoparticles in high yields,[13] whereas Pt and Au nanoparticles were poor in catalyzing this reaction. However, by suitably controlling the shape and size of the Pt and Au nanoparticles, their catalytic activity in this reaction can be enhanced. For example, a recent report[15] indicates that very small Au nanoparticles (ca. 1 nm) can catalyze the reaction in high yield (87%), but with an increase in particle size (for example, ca. 5 nm Au), the yield drops significantly to about 10%. In the case of Pt catalysts, shape control of the Pt nanoparticles enhanced the catalytic activity and the best yield obtained to date for this reaction was $14 \pm 5\%$ using octahedral Pt nanoparticles.[16] The Heck coupling reaction, on the other hand, is catalyzed by spherical Pd nanoparticles;[17] however, shape-dependent catalytic activity of Pd nanoparticles for this reaction has not been explored.

In our work, star-shaped Pt nanoflowers were demonstrated to be capable of catalyzing the Suzuki–Miyaura coupling reaction of phenyl boronic acid and iodobenzene in water in very high yield. A complete conversion (>99%) and excellent recyclability were attained; this is indeed the first demonstration of complete Suzuki–Miyaura coupling with Pt nanoflowers. Similarly, the as-prepared Pd nanoflowers were utilized to catalyze the Heck coupling reaction of styrene and iodobenzene in water. A high yield (95%) was obtained using the Pd nanoflower catalysts compared to the low yields (25%) obtained by using spherical Pd nanoparticle catalysts under comparable experimental conditions.

We utilize the pH-dependent self-assembly properties of SDBIL to synthesize nanoflowers and spherical nanoparticles of noble metals. SDBIL spontaneously forms vesicles in alkaline pH (7.0–8.5), and fibrous structures in acidic pH (5.0–6.0).[18] Relatively monodisperse nanoflowers of Au, Pt, and Pd were synthesized in high yields by mixing metal precursors and SDBIL in a 20 mM phosphate buffer of pH 5.0, followed by slow reduction with L-ascorbic acid for 24 h (for details, see the Supporting Information). The colors of Au nanoflower solutions are blue, and Pt and Pd solutions are dark brown. The UV/Vis spectra (Supporting Information, Figure S2) of

[*] Dr. A. Mohanty, N. Garg, Prof. Dr. R. Jin
Department of Chemistry, Carnegie Mellon University
Pittsburgh, PA 15213 (USA)
and
Analytical Chemistry Centre, National Metallurgical Laboratory
Jamshedpur-831007, Jharkhand (India)
E-mail: akm@nmlindia.org
rongchao@andrew.cmu.edu

[**] A.M. thanks the DST, Government of India, and CSIR, India, for a BOYSCAST Fellowship. We also acknowledge financial support from the CMU, AFOSR, and NIOSH.

Supporting information for this article is available on the WWW under http://dx.doi.org/10.1002/anie.201000902.

the Au nanoflowers exhibit two surface plasmon bands at about 580 nm and about 750 nm, which are consistent with FDTD calculations.[19] The Pt and Pd nanoflowers show essentially featureless decay curves.

The structure and morphology of the as-prepared nanoparticles were characterized by transmission electron microscopy (TEM). Figure 1 a–c shows TEM micrographs of the Pt,

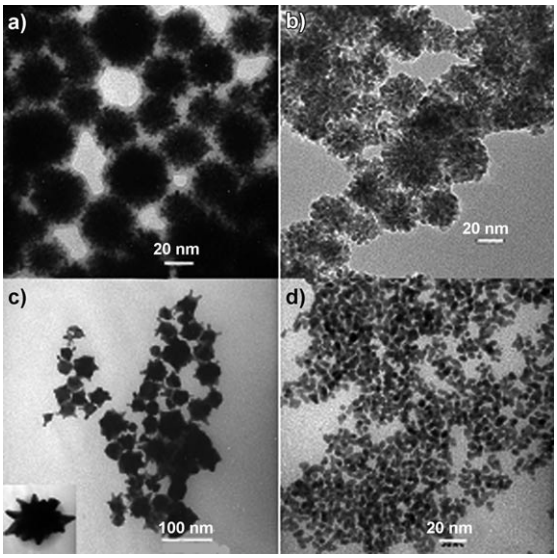

Figure 1. TEM micrographs of a) Pt, b) Pd, and c) Au nanoflowers prepared in pH 5.0 buffer, and d) spherical Au particles prepared in pH 7.5 buffer.

Pd and Au nanoparticles prepared in pH 5.0 buffer. All these nanoparticles are of a 3D flower- or star-like shape and their average diameters are (40 ± 5) nm (Pt), (25 ± 5) nm (Pd), and (50 ± 10) nm (Au). The surfaces of all the nanoflowers were very rough due to the presence of a large number of branches. A closer look at the TEM micrographs reveals that the detailed morphologies of the nanoflowers of the three metals are quite different. The average number of branches of a nanoflower is highest in the case of Pt (average ca. 100 branches), intermediate in Pd (ca. 50) and lowest in Au nanoflowers (ca. 10). And the branches of Pt nanoflowers are much thinner and smaller (1.5 nm diameter, 3–4 nm length) compared to those of Pd nanoflowers (3 nm diameter, 5–6 nm length), whilst Au nonoflowers have thick and large branches (ca. 9 nm diameter, 15–20 nm length).

The nanoflowers were further characterized by HRTEM and XRD to gain insight into the crystallinity and lattice facets present in the nanostructures. Pt nanoflowers were taken as an example. Figure 2 a shows a HRTEM image of a representative Pt nanoflower, which exhibits high contrast between the core and the peripheral branches, confirming their 3D nature. The lattice fringes are continuous from the core to the branches, revealing the high crystallinity of the nanoflowers. The SAED pattern (Figure 2 b) exhibits a diffraction pattern corresponding to {111}, {200}, {220}, and {311} lattice planes of fcc Pt. Another important observation is a diffraction ring (Figure 2 b, marked by an arrow) very

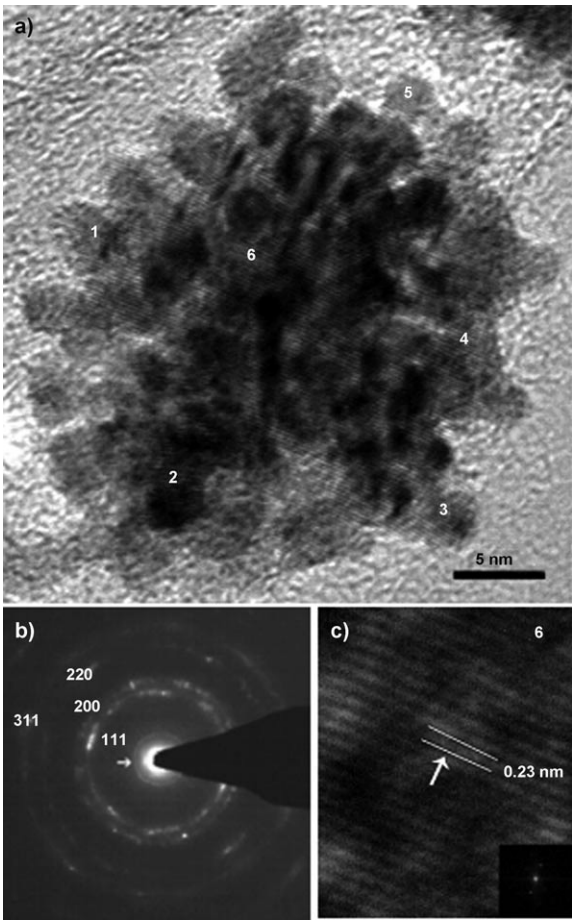

Figure 2. a) HRTEM image of a Pt nanoflower. b) SAED pattern recorded from the same nanoflower shown in (a). c) HRTEM image recorded from the center of the Pt nanoflower (marked with a 6 in (a); inset: Fourier transform of the image).

close to the central electron beam, which indicates that the nanoflower is highly textured; note that the ring was observed in all nanoflowers chosen randomly. To our knowledge, such a low-angle diffraction ring is rarely observed in TEM analysis[20] and our observation explicitly indicates a highly ordered structure of the nanoflowers. Figure 2 c and Supporting Information, Figure S3 show the HRTEM images of the different portions of the nanoflower (core and randomly selected branches, marked 1–6 in Figure 2 a). Fourier transformation of the images leads to almost identical patterns, indicating identical lattice orientation of the core and branches regardless of their different growth directions. The continuous fringes from the core to the branches of the nanoflowers suggest that the branches grow epitaxially out of the core, which rules out the possibility of random aggregates of Pt nuclei that could have formed in solution. The measured lattice spacing (0.23 nm, Figure 2 c) corresponds to {111} lattice planes of fcc Pt.

The XRD pattern of the Pt nanoflowers is shown in the Supporting Information, Figure S4. The diffraction peaks are at $2\theta = 39.4$, 46.1, 67.2, 81.1, and 85.5 degrees, corresponding to (111), (200), (220), (311), and (222) lattice planes of fcc Pt. The lattice constant (0.3919 nm) calculated from the XRD

pattern is in agreement with literature ($a = 0.3923$ nm, JCPDS 04-0802). An interesting observation is that the relative peak intensity of (200), calculated from the peak area using (111) as a reference (i.e. 100%), is identical to the literature (51% versus 53%); however, the (311) and (220) relative intensities are much higher than the standard values: 65% observed for (311) versus 33% of literature, and 50% observed for (220) versus 31% of literature. This indicates that the nanoflowers were abundant in high index {311} and {220} facets.[21,22] The Pd and Au nanoflowers also show similar structural features, as shown by TEM and XRD analyses.

We have further studied the nanoflower growth with a focus on two major factors, namely solution pH and nanoparticle growth time. Solution pH has a major influence on the growth of nanoflowers; when pH was increased from 5.0 to 7.5 whilst keeping other conditions the same, spherical particles, instead of nanoflowers, were formed. As an example, Figure 1d shows a TEM image of spherical Au nanoparticles formed in a pH 7.5 phosphate buffer. Further control experiments revealed that Au nanoflowers were formed in an acidic pH range (4.5–6.0), whereas spherical particles were formed in the alkaline pH range (7.0–8.5). The same observation was made in the cases of Pt and Pd. Using Pt as an example, we have investigated the time-dependent growth process of the nanoflowers by TEM imaging at different time intervals (Supporting Information, Figure S5). At the initial stage, nucleation occurs and small spherical particles (ca. 3 nm) are formed, followed by evolution of these nuclei to larger "seeds" (5–7 nm), which finally convert into nanoflowers (Supporting Information, Figure S5). The quasi-spherical seeds may be modeled as faceted nanocrystals such as truncated octahedra because the latter shape possesses a structural stability owing to enclosure by low-index {111} and {100} facets.[11] Lim et al. previously obtained similar single-crystalline truncated octahedral seeds of Pd by slow reduction of Na_2PdCl_4 using L-ascorbic acid to produce crystalline Pd/Pt nanodendrites.[9] In our case, the seeds are also single crystalline and act as seeding particles onto which the branches grow epitaxially to produce crystalline nanoflowers. The continuous lattice fringes from the core to branches (Figure 2a) supports the mechanism of epitaxial growth of branches on seeds and rules out random aggregation of the nuclei into nanoflowers. The Pt^{IV} ions should bind to the carboxylic group of SDBIL and are directed to the surface of the seeds. The Pt^{IV} ions are reduced to Pt^0 on the surface of the seeds, catalyzed by the Pt seed surface.[23] This process, referred to as autocatalytic growth, has been reported for the growth of various porous and branched nanostructures of different metals.[24–30] We believe that this mechanism is operating in the growth of nanoflowers because the weak reducing agent (ascorbic acid) is not strong enough to completely reduce Pt^{IV} ions to Pt^0. In the case of Au nanoflower growth, a similar mechanism is implied by the UV/Vis spectral evolution (Supporting Information, Figure S6).

The pH dependence of nanoflower formation can be explained by considering the self-assembly behavior of SDBIL. SDBIL has a tendency to slowly form long fibrous aggregates in acidic pH;[18] therefore, SDBIL can direct metal ions to deposit onto the surface of the seeds in an anisotropic manner, forming branches. In an alkaline pH, SDBIL self-assembles into spherical vesicles[18] and thus does not lead to anisotropic growth of the seeds. The necessity of SDBIL for nanoflower growth was further confirmed by our observation of no nanoflower formation using cetyltrimethylammonium bromide or sodium dodecylbenzenesulfonate as surfactants (otherwise identical conditions as the case of SDBIL). The use of a mild reducing agent, ascorbic acid, for slow reduction was found to be also critical for nanoflower formation; fast reduction using a strong reducing agent (such as $NaBH_4$) resulted in spherical nanoparticles (Supporting Information, Figure S7). The nanoflower growth rates are different for the three metals in the order Au > Pd > Pt. Owing to a faster growth, Au nanoflowers have less number of branches compared to Pt and Pd nanoflowers.

The highly dentritic nanostructures prompted us to investigate their potential catalytic properties. Nanostructures having high index facets exposed may have excellent catalytic activities because the high-index planes have a high density of atomic steps, ledges, and kinks, which serve as active sites for breaking chemical bonds.[12,31–34] We have investigated the catalytic activities of Pt, Pd, and Au nanoflowers for C–C coupling reactions (Scheme 1).

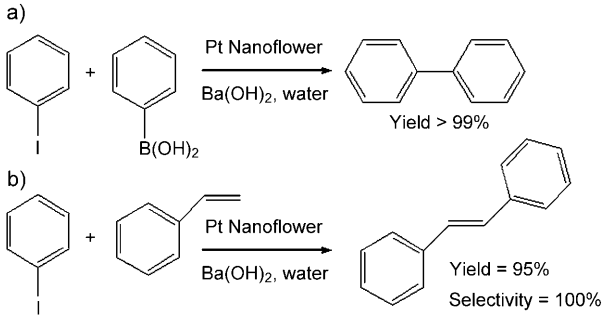

Scheme 1. a) Suzuki–Miyaura and b) Heck coupling reactions of iodobenzene with phenylboronic acid and styrene, respectively, catalyzed by nanoflowers.

The nanoflowers were first utilized to catalyze the Suzuki–Miyaura coupling reaction of phenylboronic acid and iodobenzene. A complete conversion (> 99%) was achieved when Pt nanoflowers were used as the catalyst (Table 1, entry 1). Moreover, the Pt nanoflowers were re-used for multiple cycles without any significant loss of their catalytic activity; the yield was still 95% in the sixth cycle (Supporting Information, Figure S8). This is in contrast with the results reported by El-Sayed et al.,[16] who observed a lower catalytic activity (ca. 14%) of Pt tetrahedral nanoparticle catalysts and a significant loss of activity of reused catalysts. To confirm the shape-dependent catalytic activity of the Pt nanoflowers, the coupling reaction was also performed using spherical Pt nanoparticles as the catalyst (2–3 nm in size, capped by SDBIL); the yield obtained was only 7% (Table 1, entry 2). Thus, these results clearly demonstrate the superior activity of

Table 1: Shape-dependent catalytic activity of Pt, Pd, and Au nanoparticles for Suzuki–Miyaura and Heck coupling reactions.

	Catalyst	Yield [%][c]
Suzuki–Miyaura[a]		
1	Pt, nanoflower	>99
2	Pt, spherical	7
3	Au, nanoflower	5
4	Au, spherical	0
5	Pd, nanoflower	>99
Heck Coupling[b]		
6	Pd, nanoflower	95
7	Pd, spherical	25

[a] Reaction conditions: Iodobenzene (0.2 mM), phenylboronic acid (0.4 mM), Pt nanoflower catalyst (1 mol%), $Ba(OH)_2$ (0.6 mM). [b] Iodobenzene (0.8 mM), styrene (1.0 mM), Pd nanoflower catalyst (0.2 mol%), $Ba(OH)_2$ (1.6 mM). [c] Calculated on the basis of NMR measurements (Supporting Information, Figure S9).

Pt nanoflower catalyts. Compared with spherical Pt nanoparticles, the high activity of Pt nanoflowers should be ascribed to the particular surface structure that results in more catalytically active Pt atoms on edges or corners and provides a large number of surface reaction sites. The high-index facets of nanoflowers are typically much more active than low-index facets.[31–33] Shape-dependent catalytic activity was also observed in Au nanoparticles (Table 1, entry 3). Surprisingly, Au nanoflowers catalyze the Suzuki–Miyaura coupling reaction, although the yield was low (5%). This result contrasts with spherical Au nanoparticles, which have no catalytic activity (Table 1, entry 4). As expected, Pd nanoflowers catalyze the coupling reaction in very high yields (ca. 100%; Table 1, entry 5).

The superior catalytic activity of the nanoflowers over spherical nanoparticles was also observed in Pd nanoflowers for the Heck coupling reaction of styrene and iodobenzene in water (Scheme 1). A high yield (95%) of *trans*-stilbene was obtained using nanoflowers, in contrast to the moderate yield of 25% when spherical Pd nanoparticles capped by SDBIL were used (Table 1, entry 6 and 7). An almost 100% selectivity for *trans*-stilbene was observed in both cases. Wai et al. previously reported a 94% yield for the same Heck coupling reaction using carbon nanotube supported Pd nanoparticles and 53% conversion using commercial Pd/C catalyst (10 wt% Pd, Aldrich).[34] We also performed blank experiments for the catalytic reactions using SDBIL only; no catalytic reaction was observed, confirming that the catalysis originates in the metal nanoparticles.

In summary, we have devised a universal approach for high yield synthesis of nanoflowers of Au, Pt, and Pd using SDBIL surfactant. The pH-dependent self-assembly of SDBIL is critical for the growth of the nanoflowers, which have a crystalline fcc structure with ample high-index facets. The Pt nanoflowers have superior catalytic activity (>99% yield) for the Suzuki–Miyaura and also the Heck coupling reactions. The nanoflowers also hold promise in other important reactions, such as oxygen reduction in fuel cells.[35]

Received: February 12, 2010
Published online: June 10, 2010

Keywords: gold · heterogeneous catalysis · nanostructures · palladium · platinum

[1] a) Y. Xia, Y. Xiong, B. Lim, S. E. Skrabalak, *Angew. Chem.* **2009**, *121*, 62–108; *Angew. Chem. Int. Ed.* **2009**, *48*, 60–103; b) C. Burda, X. Chen, R. Narayanan, M. A. El-Sayed, *Chem. Rev.* **2005**, *105*, 1025–1102; c) J. E. Millstone, W. Wei, M. R. Jones, H. Yoo, C. A. Mirkin, *Nano Lett.* **2008**, *8*, 2526–2529; d) C. Salzemann, W. Zhai, N. Goubet, M.-P. Pileni, *J. Phys. Chem. Lett.* **2010**, *1*, 149–154.
[2] L. Rodríguez-Lorenzo, R. A. Álvarez-Puebla, F. J. García de Abajo, L. M. Liz-Marzán, *J. Phys. Chem. C* **2009**, DOI: 10.1021/jp909253w.
[3] G. C. Khoury, T. Vo-Dinh, *J. Phys. Chem. C* **2008**, *112*, 18849–18859.
[4] B. K. Jena, C. R. Raj, *Langmuir* **2007**, *23*, 4064–4070.
[5] Q. Wei, H. M. Song, A. P. Leonov, J. A. Hale, J. D. Oh, Q. K. Ong, K. Ritchie, A. Wei, *J. Am. Chem. Soc.* **2009**, *131*, 9728–9734.
[6] M. A. Mahmoud, C. E. Tabor, M. A. El-Sayed, Y. Ding, Z. L. Wang, *J. Am. Chem. Soc.* **2008**, *130*, 4590–4591.
[7] Z. Yin, H. Zheng, D. Ma, X. Bao, *J. Phys. Chem. C* **2009**, *113*, 1001–1005.
[8] S. Sun, D. Yang, D. Villers, G. Zhang, E. Sacher, J. P. Dodelet, *Adv. Mater.* **2008**, *20*, 571–574.
[9] a) B. Lim, M. Jiang, P. H. C. Camargo, E. C. Cho, J. Tao, X. Lu, Y. Zhu, Y. Xia, *Science* **2009**, *324*, 1302–1305; b) B. Lim, M. Jiang, T. Yu, P. H. C. Camargo1, Y. Xia, *Nano Res.* **2010**, *3*, 69–80.
[10] a) K. M. Bratlie, C. J. Kliewer, G. A. Somorjai, *J. Phys. Chem. B* **2006**, *110*, 17925–17930; b) K. M. Bratlie, H. Lee, K. Komvopoulos, P. Yang, G. A. Somorjai, *Nano Lett.* **2007**, *7*, 3097–3101.
[11] a) C. Wang, H. Daimon, T. Onodera, T. Koda, S. Sun, *Angew. Chem.* **2008**, *120*, 3644–3647; *Angew. Chem. Int. Ed.* **2008**, *47*, 3588–3591; b) Y. J. Xiong, J. M. McLellan, Y. D. Yin, Y. N. Xia, *Angew. Chem.* **2007**, *119*, 804–808; *Angew. Chem. Int. Ed.* **2007**, *46*, 790–794; c) H. Song, F. Kim, S. Connor, G. A. Somorjai, P. Yang, *J. Phys. Chem. B* **2005**, *109*, 188–193; d) F. Baletto, R. Ferrando, A. Fortunelli, F. Montalenti, C. Mottet, *J. Chem. Phys.* **2002**, *116*, 3856–3863.
[12] a) M. S. Bakshi, *J. Phys. Chem. C* **2009**, *113*, 10921–10928; b) L. Wang, Y. Yamauchi, *J. Am. Chem. Soc.* **2009**, *131*, 9152–9153.
[13] K. Sawai, R. Tatumi, T. Nakahodo, H. Fujihara, *Angew. Chem.* **2008**, *120*, 7023–7025; *Angew. Chem. Int. Ed.* **2008**, *47*, 6917–6919.
[14] L. Djakovitch, K. Kohler, J. G. de Vries in *The Role of Palladium Nanoparticles as Catalysts for Carbon–Carbon Coupling Reactions in Nanoparticles and Catalysis* (Ed.: D. Astruc), Wiley-VCH, Weinheim, **2008**, pp. 303–348.
[15] J. Han, Y. Liu, R. Guo, *J. Am. Chem. Soc.* **2009**, *131*, 2060–2061.
[16] R. Narayanan, M. A. El-Sayed, *J. Phys. Chem. B* **2005**, *109*, 12663–12676.
[17] J. Durand, E. Teuma, M. Gomez, *Eur. J. Inorg. Chem.* **2008**, 3577–3586.
[18] A. Mohanty, J. Dey, *Langmuir* **2007**, *23*, 1033–1040.
[19] F. Hao, C. L. Nehl, J. H. Hafner, P. Nordlander, *Nano Lett.* **2007**, *7*, 729–732.
[20] P. E. Champness in *Electron Diffraction in Transmission Electron Microscope*, BIOS Scientific Publishers, Oxford, UK, **2001**, pp. 120–125.
[21] Y. Sun, Y. Xia, *Science* **2002**, *298*, 2176–2179.
[22] B. D. Cullity, S. R. Stock in *Elements of X-ray Diffraction*, 3rd ed., Prentice-Hall, Upper Saddle River, NJ, **2001**.
[23] L. Colombi Ciacchi, W. Pompe, A. D. Vita, *J. Phys. Chem. B* **2003**, *107*, 1755–1764.
[24] A. Henglein, *Chem. Rev.* **1989**, *89*, 1861–1873.

[25] Y. Song, Y. Yang, C. J. Medforth, E. Pereira, A. K. Singh, H. Xu, Y. Jiang, C. J. Brinker, F. van Swol, J. A. Shelnutt, *J. Am. Chem. Soc.* **2004**, *126*, 635 – 645.
[26] J. Chen, T. Herricks, Y. Xia, *Angew. Chem.* **2005**, *117*, 2645 – 2648; *Angew. Chem. Int. Ed.* **2005**, *44*, 2589 – 2592.
[27] X. Teng, X. Liang, S. Maksimuk, H. Yang, *Small* **2006**, *2*, 249 – 253.
[28] B. Lim, X. Lu, M. Jiang, P. H. C. Camargo, E. C. Cho, E. P. Lee, Y. Xia, *Nano Lett.* **2008**, *8*, 4043 – 4047.
[29] E. E. Finney, R. G. Finke, *J. Colloid Interface Sci.* **2008**, *317*, 351 – 374.
[30] L. C. Ciacchi, M. Mertig, R. Seidel, W. Pompe, A. De Vita, *Nanotechnology* **2003**, *14*, 840 – 848.
[31] R. Narayanan, M. A. El-Sayed, *Nano Lett.* **2004**, *4*, 1343 – 1348.
[32] N. Tian, Z.-Y. Zhou, S.-G. Sun, Y. Ding, Z. L. Wang, *Science* **2007**, *316*, 732 – 735.
[33] G. A. Somorjai, D. W. Blakely, *Nature* **1975**, *258*, 580 – 583.
[34] B. Yoon, C. M. Wai, *J. Am. Chem. Soc.* **2005**, *127*, 17174 – 17175.
[35] J. Wu, J. Zhang, Z. Peng, S. Yang, F. T. Wagner, H. Yang, *J. Am. Chem. Soc.* **2010**, *132*, 4984 – 4985.

